Materials Characterization Techniques—Principles and Applications
Eds : G. Sridhar, S. Ghosh Chowdhury & N. G. Goswami
© NML, Jamshedpur-831007 (1999) pp. 69-90

Principles of Microscopy

S. R. SINGH
National Metallurgical Laboratory, Jamshedpur - 831 007
E-mail : srsingh@csnml.ren.nic.in

ABSTRACT

The microstructural characterization by microscopic techniques is an essential requirement for materials design as well as materials performance. This paper, starting from historical developments of microscopy, deals with the various methods of optical microscopy, transmission electron microscopy and scanning tunneling microscopy. In optical microscopy emphasis have been given to multiple beam interferometry (MBI) capable of achieving the vertical resolution of 1 nm while lateral resolution remains to that of optical microscopy. It's capability to unmask microtopographies of surfaces is illustrated by few industrial examples. The operating principles of transmission electron microscopy alongwith various imaging modes illustrated with examples have been described. The capability of Moire fringe in imaging of nanoparticles have been highlighted. The Lorentz microscopy in Fresel imaging and coherent Foucault imaging modes are capable of providing quantitative information about magnetic properties/ substructures. The generic concept of scanning tip microscopies utilizing some physical property of probe-sample interaction have been described.

INTRODUCTION

In order to understand the response of metals and alloys to static, dynamic and cyclic stresses, various environments and temperatures, it is essential to be able to describe the "total microstructure". For this it may be necessary to combine the knowledge of chemical composition, crystal and defect structure, and the proportion and distribution of various phases present. This branch of science dealing with the microstructure of metals and alloys is called metallography.

The fundamentals of microstructural investigations of metals and alloys were laid over a hundred year ago by Henry Clifford Sorby who developed a preparation method and etching treatment for viewing metal samples under reflected light microscope. Indeed it is this technique, progressively refined, which remains a powerful tool to the metallogrpher for establishing essential microstruc-

tural features such as grain size and shape and distribution of phases to the limit of resolution of the optical microscope ~ 3000 Å. The development in early 1950's of a theoretical understanding of the principles controlling the strength of materials resulted in a need to consider techniques with resolution approaching that of an interatomic spacings. This lead to use of electrons where the shorter wavelengths enable resolutions of ~ 2 Å to be achieved with current generation of electron microscopes. The application of current generation of electron microscope, capable of resolving atomic columns, in study of materials seems to be the historical consequences of a long succession of discoveries and inventions collated in table 1. In general, the microscopy should be considered as part of human's unending efforts to see, with better clarity and in increasing detail, the material world in which we live and of which we form a so small a part. This leads to a steady increase in the delicacy and extent of our sensory perceptions. This extension of vision have the special value that arises from the directness with which their information can be interpreted.

The broadly classified techniques used for microstructural studies are as follows: (1) Optical microscopy. (2) X-ray topography. (3) Scanning electron microscopy (SEM) (4) Transmission electron microscopy (TEM). (5) Analytical electron microscopy and (6) Scanning tunneling microscopy. In this article, the principles supplemented by appropriate examples of optical microscopy, transmission electron microscopy and scanning tunneling microscopy techniques are described. Certainly techniques are reaching a stage where potentially it is possible to establish the information necessary to correlate existing theoretical models describing high and low temperature deformations and fracture, corrosion, oxidation, environmentally assisted fracture, electrical and other physical properties with the material microstructure.

OPTICAL MICROSCOPY

Properties of the Objective Lens

The objective lens system which forms the primary image of the specimen is the most important part of an optical microscope. An understanding of the optical properties is essential to the correct selection of an objective for a specific purpose.

Numerical Aperture : Numerical aperture (NA) of the objective is a measure of the light collection function and is defined as;

$$NA = \mu \, Sin\alpha \qquad ...(2.1)$$

where μ is the refractive index of the medium between specimen and the objective lens, α, the semi angle of the most oblique rays entering the front of the objective. For example, a dry lens (air medium between objective and specimen,

$\mu = 1$) has NA < 1, while oil immersion lens with cedar wood oil and monobromonapthalene has NA = 1.3 and 1.6 respectively. The effective NA of the microscope is defined as;

$$NA_{effective} = \frac{(NA_{objective} + NA_{condenser})}{2} \qquad (2.2)$$

where $NA_{condenser} \geq NA_{objective}$.

Table 1: History and development of microscopy

1839 :	L. Daguerre's invention of silver plate method of optical microscope.
1850 :	(1) Metallography - optical microscope and photography after invention of Daguerre.
	(2) Development of optical microscopy supported by L. Seidel's theory of lens aberrations.
1864 :	H. C. Sorby - First microscopic observation of steel (Magnification < 10x).
1880 :	Abbe's oil immersion method (Magnification ≈ 2000x).
1924 :	L. de Broglie - Theoretical prediction of the "material wave" (wave-particle duality).
1926 :	H. Busch - Design of electric field and magnetic-field lens for an electron beam.
1927 :	C. J. Davisson and L. H. Germer - discovery of electron diffraction.
1928 :	H. Bethe - Dynamical diffraction theory. Application to microscope image contrast was made later in 1961 by A. Howie and M. J. Whelan.
1931 :	M. Knoll - Possibility for the construction of an electron microscope.
1932 :	M. Knoll and E. Ruska - First paper using the word Elekronenmikroskop".
1938 :	B. von Borries and E. Ruska-TEM quite similar in basic features as of today's TEM was built.
1950 :	(1) R. Castaing: precipitation in age-hardenable Al-alloys. Around 1950 studies of metals by surface replica combined with metallographic etching.
	(2) Improvements in thinning method.
1956 :	W. Bollmann and P. B. Hirsch et al. -Succeeds in observing dislocations in metal crystals. (Dislocation images ~ 10 nm).
1956 :	J. W. Menter - Lattice plane imaging. (d = 11.9 Å).
1960 :	P. B. Hirsch - Image contrast theory.
1961 :	A. Howie and M. J. Whelan - Application of Bethe's theory.
1969 :	D. J. H. Cockayne - Weak beam method. (Dislocation images ~ 2 nm).

Resolution : Resolution is a function of NA, wavelength and coherency of the light. The limit of resolution, i.e., the maximum distance which may just be resolved is given by Abbe as;

Limit of Resolution = 0.5 λ / NA (for coherent illumination) ...(2.3)

Resolving Power = 1 / limit of resolution = 2 x NA / λ ...(2.4)

whereas for incoherent illumination e.g., in fluorescence microscopy,

Limit of Resolution = 0.61λ / NA ...(2.5)

Resolving Power = NA / 0.61λ ...(2.6)

Figures 1 and 2 illustrate the effect of wavelength and numerical aperture respectively on the resolution.

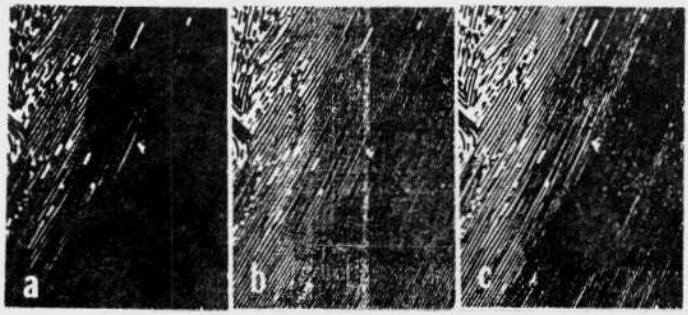

Fig. 1 : The effect of wavelength upon resolution obtained with a particular objective (NA=1.4). Pearlite structure, x1800. (a) Partially resolved (λ=6800 Å), (b) more completely resolved (λ=5500 Å), (c) even more completely resolved (λ=4700 Å).

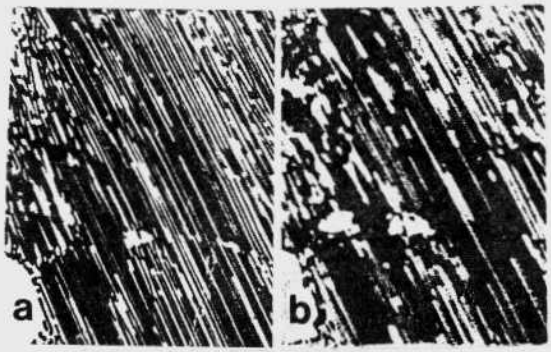

Fig. 2 : Effect of NA upon resolution. Pearlite structure, x1500. (a) NA=1.25 (b) NA=0.65.

Magnification: The magnification of an optical system is the ratio of numerical aperture on object side to numerical aperture on the image side i.e., $M = (NA)_{obj} / (NA)_{img}$. The total magnification of the compound microscope for visual observation is given by,

$$M_t = M_o \times M_e \qquad ...(2.7)$$

whereas the magnification for the projection microscope is,

$$M_p = (M_o \times M_e \times M_r \times D) / 250 \qquad ...(2.8)$$

where, M_o and M_e are initial magnifications of objective lens and the eyepiece, M_r is the magnification of relay or zoom system if any and D is projection distance between eyepiece to film plane. The total magnification of the microscope has practical upper and lower limits. The lower limit of total magnification for an objective lens results from the finite limit of resolution of eye, which is greater than 1 minute of arc. If the image is presented at a distance of 250 mm, the minimum magnification required to visually resolve the images of two particles which are just resolved by the objective is given by,

$$Mag_{min} = \frac{\text{Minimum distance between particles resolved by eye.}}{\text{Minimum distance between particles resolved by the microscope.}}$$

$$= (2 \times NA \times \tan 1' \times 250) / \lambda \qquad ...(2.9)$$

$$\approx 300\ NA \text{ (for } \lambda = 5000\ Å)$$

Therefore, for a 10 power lens with a NA of 0.25 (written as 10x /0.25) the $Mag_{min} = 300 \times 0.25 = 75x$. Using equation (2.7), we can see that at least an 8x eyepiece would be required to permit the eye to resolve the finest structure resolvable with this objective. For easier viewing the magnification may be increased to 1000 NA without seriously affecting the image quality. The upper limit of total magnification is usually considered to be about 1000 NA. The magnification above this value is possible but the resolution is not increased. This condition is referred as "empty magnification".

Image Brightness : The resolution of the objective is dependent on the numerical aperture on the object side of the lens system, image brightness is governed by the numerical aperture on the image side. This relationship is depicted Fig. 3.

The NA in the image space is given by ;

$$NA_I = NA_{obj} / M_o \qquad ...(2.10)$$

The image brightness, B_I is then proportional to $(NA_I)^2$

$$\text{i.e., } B_I \propto (NA_I)^2 \qquad ...(2.11)$$

As a comparative example, the brightness for a 16x/0.25 objective is about three times as great as for a 150x/1.40 objective.

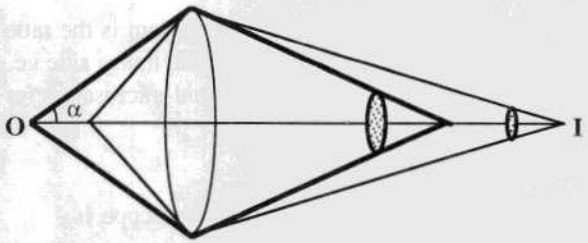

Fig. 3 : The relationship between optical side NA and resolution, and between image side NA and brightness. O is the object side, α is the half angle of most oblique ray entering the objective lens.

Depth of Field: is the distance along the optical axis over which details of the object can be observed with adequate sharpness. Factors affecting resolving power influence depth of field as well in opposite direction, i.e., increasing the resolving power decreases the depth of field. The depth of field (T_f) is given by;

$$T_f = \frac{\lambda \sqrt{(\mu^2 - NA^2)}}{2\ NA^2} \qquad \ldots (2.12)$$

since the object plane can be moved both above and below the plane of focus, therefore the actual depth of field is $2T_f$.

Mode of Examination in Optical Microscopy

The image contrast in an optical micrograph can be improved by developing differential local coefficient of scattering and reflection through polishing and etching. The optical methods for enhancing contrast applicable to any kind of surface condition are;

- Bright-field illumination.
- Oblique illumination.
- Dark-field illumination.
- Polarized light.
- Phase contrast illumination.
- Multiple beam interferometry.
- Interference contrast illumination.

An optical ray diagram of vertical illumination microscope is shown in Fig. 4 while Fig. 5 depicts bright-field, oblique and dark-field illumination. The bright-field illumination makes maximum use of the numerical aperture (NA) available. The oblique and dark-field illumination reduces the NA of objective thereby degrading the attainable resolution while increasing the overall contrast and relief effect of surface features. In the polarized light illumination a polarizer is placed into the condenser system of an optical microscope and a second polarizer (called analyzer) is positioned between the objective lens and the eye piece. The polarizer and analyzer causes a phase change in direct beam reflected from an anisotropic material. This aid in identification of different phases.

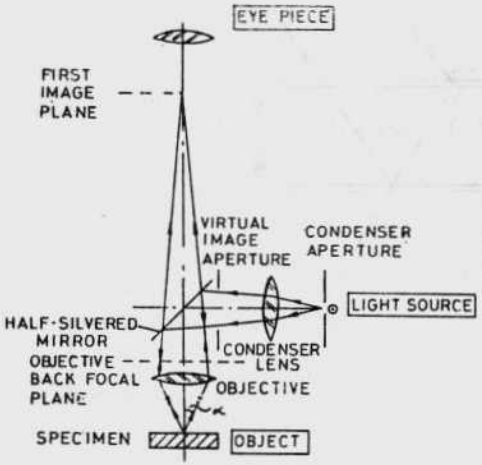

Fig. 4 : Ray diagram of vertical illumination optical microscope.

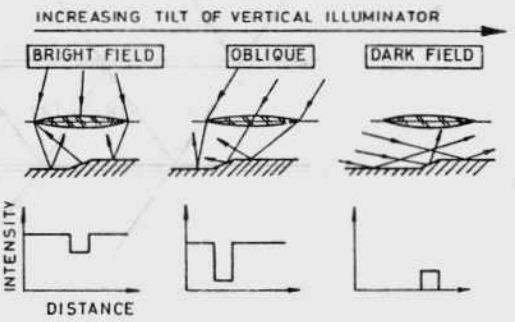

Fig. 5 : Bright-field, oblique and dark-field illumination together with corresponding image intensity distributions showing progressive enhancement of image feature.

Multiple Beam Interferometry : Multiple beam interferometry (MBI) is a powerful tool for unmasking the subtle microtopographies which exist both on natural surfaces and on those exposed to some treatment or other. It is completely a non-destructive method and possible to achieve a vertical resolution of upto 5 Å. It reveals and measures the microcontours of grown metal surfaces as well as treated surfaces i.e., coating, deformation, distortion, corrosion. The high magnification and resolution in interference fringes refer only to the up-down direction while across the lateral extension, the magnification characteristic of an ordinary optical microscope operate.

A simplified theory which is not essential for practicener is outlined and depicted schematically in Fig. 6. AB and CD are two silvered parallel plates distance t apart and let parallel light from source S is incident at an angle θ on AB. At point a on AB the reflected and transmitted fractions are R and T respectively. Assuming unit incident intensity and neglecting absorption lead to relation $R + T = 1$. It is assumed, for simplicity, that similar fractions are reflected at CD. The multiply reflected beams at a, b, c, d, e, etc. can be collected by lens either in reflection or in transmission and gives rise to interference fringes in either case at the lens focus. The light beams form a diminishing series in which the intensities diminish geometrically whilst, because of parallelism, path lengths increase arithmetically. The successive transmitted beams have intensities which sums up to make the series,

$$T^2 + R^2T^2 + R^4T^2 + R^6T^2 + \ldots \qquad \ldots (2.13)$$

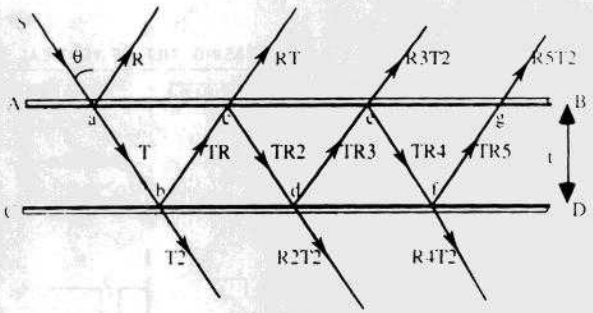

Fig. 6 : Schematics showing amplitude and path difference of multiple reflected beams between two reflecting planes AB and CD.

The path difference between two successive beams is 2t Cosθ, and corresponding the phase difference (δ) = ($4\pi t$ Cosθ)/λ The intensity distribution due to interference of successive transmitted beams is given by Airy,

$$I_T = \frac{[\ T / (1-R)]^2}{[\ 1 + \{4R / (1-R)^2\}\ \mathrm{Sin}^2(\delta/2)\ ]} \qquad \ldots (2.14)$$

The Airy conditions is realized only when the separation between the surfaces is very small, preferably of the order of a light wavelength. Since, T + R + A =1, if we neglect the absorption, then, T + R = 1, therefore intensity is given by,

$$I_T = \frac{1}{[\ 1 + \{4R / (1-R)^2\}\ \mathrm{Sin}^2\ (\delta/2)\ ]} \qquad \ldots (2.15)$$

The resulting fringe shape is determined solely by the value of [4R / $(1-R)^2$] which is called the coefficient of finesse (F). Therefore intensity is given by,

$$I_T = \frac{1}{1 + F\ \mathrm{Sin}^2(\delta/2)} \qquad \ldots (2.16)$$

As R approaches unity, fringes becomes very narrow. The fringe half-width i.e., fringe width at half maximum is given by,

Fringe half-width = 0.63 / $F^{1/2}$.

For R = 0.75, half-width = 1/11 of an order.

For R = 0.95, half-width = 1/61 of an order.

For R = 0.97, half-width = 1/104 of an order.

Similarly the intensity distribution due to interference of successive reflected beams is given by,

$$I_R = \frac{F\ \mathrm{Sin}^2\ (\delta/2)}{[1 + F\ \mathrm{Sin}^2\ (\delta/2)]} \qquad \ldots (2.17)$$

The interference patterns in reflection and transmission are complimentary to each other, in the sense that, $I_T + I_R = 1$. The intensity distribution in reflected light is shown in Fig. 7, where dark fringes are separated by bright background.

Reflecting Materials Coating : The coating can be performed by resistive evaporation of coating material on substrate or sample, as required, in a vacuum coating unit operating at 10^{-6} torr. Silver deposition contours effectively perfect on the low magnification scale of the optical microscope. The thickness of silver film should be maintained about 700 Å. The examination of steel sample preferably requires a hard coating on the flat glass substrate. This can be achieved by coating a quarter wave thickness of rutile (TiO_2), i.e., ~ 500Å for use with mercury green light of wavelength 5460 Å. The composite reflectivity of rutile on glass and steel sample gives a coefficient of finesse (F) of about 6 which produces a moderately narrow fringes. For very high reflectivity, coating of dielectric multilayers consisting of successive layers of ZnS (μ = 2.36) and cryolite (μ = 1.36) each of quarter wave thickness gives virtually negligible absorption for visible light. The multilayer reflectivities (R) of 0.94, 0.97 and 0.99 can be achieved by coating 7 layers, 9 layers and 21 layers respectively.

Measurement of topographical features : The fringes produced correspond to contour of equal thicknesses. Therefore, a parallel plate configuration of reference flat glass and sample produces straight fringes. Any deviation from parallelism is reflected in the curvature of the fringes as well as shift of fringe orders. Each fringe order separation indicate a change in height corresponding to one wavelength as depicted in Fig. 8. Therefore the dispersion of fringes depends on the wedge angle of the film. The following types of measurement can be done on interferograms;

(1) Radii of curvature of spherical hills and valleys.

(2) Depth and height of ruts and ridges.

(3) Angle of inclination between roof tops.

(4) Inclines and slopes.

(5) Discontinuous steps.

(1) Radii of curvature of spherical hills and valleys: Radius of curvature (R) of the object is;

$$R = \frac{(r^2_m - r^2_n)}{(m-n)} \cdot \frac{1}{\lambda M^2} \qquad \ldots (2.18)$$

where r_m and r_n are the radii of rings numbered m and n, and M is the linear magnification. A plot between r^2 and ring number is a straight line with slope of $R\lambda M^2$, from which R can be evaluated. A deviation from straight line indicates the deviation from sphericity. The fringe pattern from a solid sphere refers to hill.

A slight pressure on the sample lead to outward movement of fringes while movement towards center indicate presence of hollow (valley). These are schematically represented in Fig. 9. Figures 10 (a&b) show the application of interferometric method in assessing the surface defects on a spherical object (e.g., ball-bearing). In Fig 10a, the fringes are far from circular, especially noticeable in the inner rings. Also local defect is a circular hollow, as indicated by direction of fringe displacement. Furthermore, it is almost one fringe deep. Fig. 10b shows more distorted fringe pattern which results when a ball-bearing is subjected to excessive load.

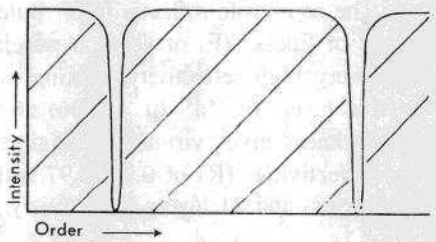

Fig. 7 : Intensity distribution in the interference pattern obtained in reflection.

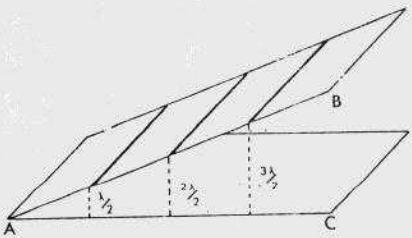

Fig. 8 : Fringes of equal thickness obtained in the wedge film.

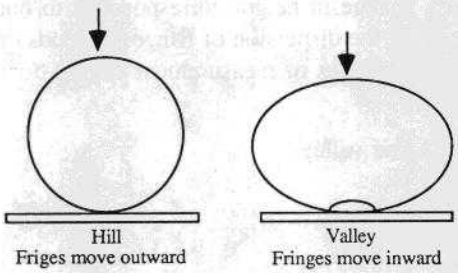

Fig.9: Schematics showing identification of hill and valley by movement of fringes.

Fig. 10: Interferograms of ball-bearing with, (a) manufacturing defect, (b) distortion due to overloading.

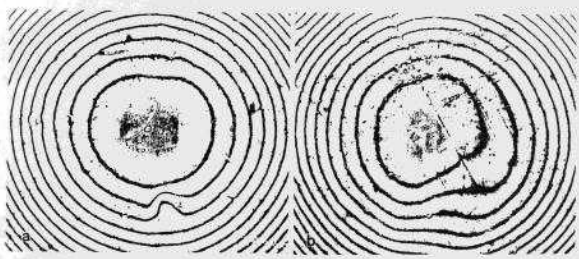

(2) Depth and height of ruts and ridges: The presence of ridges and ruts give rise to local deviation in fringe profile which is illustrated in Fig. 11.

$$\text{Size of the feature} = X\,\lambda\,/\,(CE + EG) \qquad \ldots (2.19)$$

(3) Angle measurements: This must be borne out in mind that angles are magnified in interferometry. The fringe orientation on either side of roof top is only a question of tilt of the optical flat.

$$\text{The angle made by the surface} = (\lambda/2).(1/x) \qquad \ldots (2.20)$$

where x is the magnification on the original surface. As an example the interferogram recorded at optical magnification of 100x, showing 2 cm broad band (Fig. 12). The magnification on original surface is 2/100 or 1/50 = x. Therefore the band containing 15 fringes represents an angular slope of $15.(\lambda/2).(1/x) = 15*2730*50*10^{-8} \sim 1°$. The number of fringes intercepted per centimeter gives the hill slope in the selected direction.

(4) Abrupt Steps: Abrupt steps appear on crystalline cleavage faces and growth faces. In Fig. 13, the upper set of fringes A_1, A_2... and lower set of fringes B_1, B_2... are separated by quantities x_1, x_2... due to fringe shift at the step. The step height at any region, say A_2B_2, is given by;

$$\text{Step height} = x_2\,\lambda\,/\,\{(B_1 - B_2) + (A_2 - A_3)\} \qquad \ldots (2.21)$$

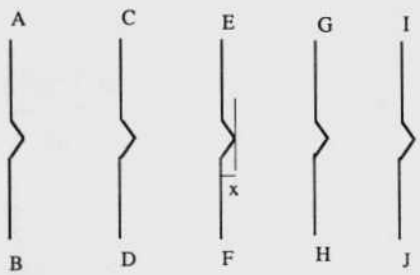

Fig. 11: Measurement of height (or depth) associated with a displacement "X" in a fringe pattern.

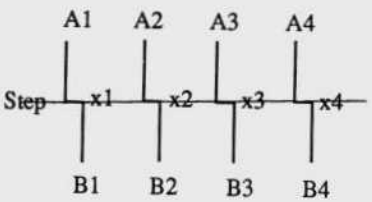

Fig. 13: Schematic of discontinuity in fringe pattern due to abrupt step.

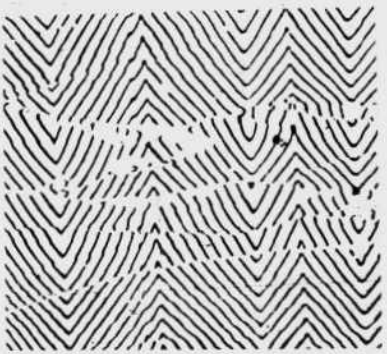

Fig. 12 : Interferogram showing surface microtopography containing cleavage steps on a single crystal of bismuth.

Interference contrast microscopy : Suppose two silvered parallel plane plates are illuminated at normal incidence with parallel light of wave length λ For incident intensity I_o, the transmitted intensity I_T depends on the plate separation t as discussed in the previous section and given by Eq. 2.16,

$$I_T = I_o /[1 + F \sin^2(\delta/2)]$$

where $\delta/2$ is $2\pi t/\lambda$, and coefficient of finesse F is $4R/(1-R)^2$, R being the reflectivity. If the separation t is continuously altered the transmitted intensity varies as depicted in Fig. 14a, where each maxima is due to change in t of $\lambda/2$. In a minimum region (halfway between peaks), a small change dt makes no effective alteration in I. Not so if t be selected so that a small change dt in thickness produces a very big change dI in intensity. If we assume 10% change in intensity is visually detectable, then fraction of an order which will produce this 10% change is;

$$dt = \lambda / 20 \pi F^{1/2} \qquad \ldots (2.22)$$

For R = 0.97, dt = 1.5 Å. Therefore, if we have two near plane parallel surfaces and arrange to adjust t to optimum position, then the undulations of mere crystal lattice dimension will show themselves as a region of observable different intensity. There is thus enormous enhancement in contrast, as illustrated in the micrograph taken from high quality diamond (Fig.14b).

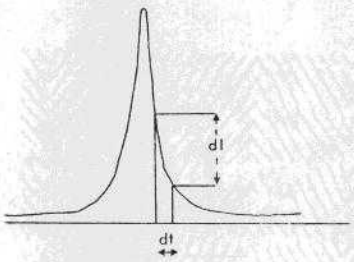

Fig. 14 : (a) Variation of transmitted intensity with contact gap in interference contrast microscopy.

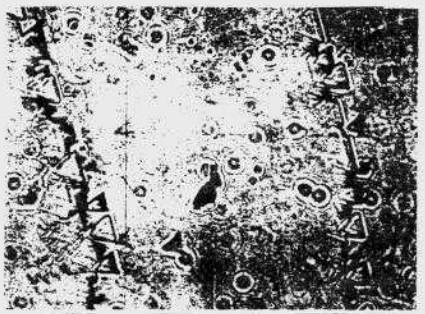

14 (b) : Interference contrast on a diamond surface

The multiple beam interference contrast has advantage over Zernike's phase contrast for the following reasons. The origin of Zernike contrast is through diffraction. It therefore shows up vividly for sharp edges and boundaries and also for any very close grain structure which produces adequate diffraction. It fails for coarse region or smoothly varying (curved or lenticular) regions, which are not effective diffracting agents. In contradistinction, interference contrast does not

fail on extended regions. Partial obstruction of the lens can often lead to quite awkward strong diffraction halo artifact in phase contrast microscopy while no such artifact occur in interference contrast microscopy.

Phase contrast illumination : A phase object alters the phase but not the amplitude of incident wave. An object of this type is of non-uniform optical thickness (μt) but does not absorbs any of the incident light. Eye or an observing instrument only distinguishes the change in intensity (amplitude disturbances in the image plane). One can only draw conclusion about the amplitude changes but not about the phase changes introduced by the object. Information about phase objects can be obtained by : (1) central dark ground method of observation, where the central order is excluded by a stop, or, (2) Schlieren method, where all the spectra on one side of the central order are excluded, and, (3) Zernike phase contrast, which has the advantage that it produces an intensity distribution which is directly proportional to the phase changes introduced by the object, and is achieved by introducing quarter wave plate in the path of the central order.

TRANSMISSION ELECTRON MICROSCOPY

Since the majority of techniques used to examine the microstructure involves use of certain kinds electromagnetic radiation, generally speaking, all these methods are based upon some interaction of matter with radiation of different kinds. The various radiations used for microstructural studies and their mode of observation are collated in table 2.

Table 2

Nature of radiation		*Method of observation*	
Particles	Wave-length		
X-ray photons	1Å		Diffraction
Electrons (high energy)	0.05Å	Microscopy	Diffraction
Electrons (low energy)	1Å		Diffraction
Neutrons	1 - 10Å		Diffraction
Ions		Microscopy	

The elastic scattering cross section varies as inverse square of beam energy, therefore, the rate of elastic scattering per unit path length rapidly decreases as the beam energy increases. This reduction in elastic scattering cross section with increasing beam energy is being utilized in thin foil TEM. In the thin foil, as opposed to bulk SEM sample, the elastic scattering is greatly reduced if the thickness is comparable to the mean free path of elastic scattering. It is appropriate to consider some theoretical concepts on which transmission electron microscopy is based.

Resolution :

For a simple general optical system, applying the Rayleigh criterion to the Abbe's formulation defines the resolution for optical microscopy since this is limited by diffraction of each point within the object which is spread into small disc (Airy disc) in the image. Thus the resolving power, δ, is given by

$$\delta = k\lambda / \mu \sin\alpha \qquad ...(3.1)$$

where λ is the wavelength, μ, the refractive index of medium, α, is semiangle subtended by object at the lens and k is a constant usually taken to be 0.61, depending on coherence of illumination. For an optical microscope with white light illumination ($\lambda \approx 5000$ Å) fitted with an oil immersion lens ($\mu \sin\alpha = 1.35$) it is possible to achieve a resolution of about 2000 Å. In the case of electrons, the de'Broglie relationship,

$$\lambda = h / p \qquad ...(3.2)$$

relates the wavelength of electron, λ, to their momentum p, and Planck's constant h. If the electrons are accelerated by a potential difference of V volts then,

$$\lambda = h / \sqrt{(2meV)} \qquad ...(3.3)$$

where m and e is the mass and charge of the electrons respectively. Many of the current electron microscopes operate with voltages in the range of 100 to 300 kV which corresponds to electron wavelength of 0.037 Å to 0.0197 Å. Spherical aberration is the main factor which limits the performance of electromagnetic lenses used in microscope and results in α being kept small in equation (3.1). The resolving power is,

$$\delta \sim \lambda^{3/4} C_s^{1/4} \qquad ...(3.4)$$

Therefore for TEM operating at 200 kV, with $\lambda = 0.0251$ Å and $C_s = 2$mm, the limit of resolution ~ 2.7 Å. In deciding the achievable resolution one must consider the other lens defects such as astigmatism, distortion, chromatic aberration, etc.

Diffraction

When either x-rays or electron interact with a crystalline material they are subject to diffraction which, for monochromatic radiation, produces a series of strongly diffracted beams leaving the crystal in defined and predicted directions. The relationship between the crystal lattice, the incident radiation and the resultant diffraction pattern is given by Bragg's law

$$n\lambda = 2d \sin\theta \qquad ...(3.5)$$

where λ is the wavelength of incident radiation, d is the spacing between specific crystal planes which makes an angle θ with the incident radiation and n is an integer. The conditions for diffraction using the concept of reciprocal lattice is shown in Fig. 15 and given by,

$$\mathbf{g} = \mathbf{k}_1 - \mathbf{k}_0 \qquad ...(3.6)$$

where **g** is the reciprocal lattice vector corresponding to diffracting planes, $\mathbf{k}_0$ is the incident wave vector (=1/λ), k_1 is the diffracted wave vector and **s** is the deviation parameter. The intensity in $\mathbf{k}_1$ and $\mathbf{k}_0$ oscillates with thickness and the oscillation depth is governed by the extinction distance ξ_g. The ξ_g is proportional to relativistic mass m which increases 2.5 times between 100 kV and 1 MV while the wavelength λ decreases by ~ 4.3 times, which means that the radius of reflecting sphere increases by the same factor. Therefore more reciprocal lattice points are intersected by the reflecting sphere at high voltages leading to multiple beam conditions. The so called two beam condition is considered optimum for traditional 100 kV microscopy.

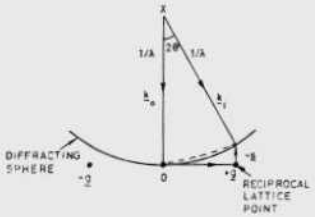

Fig. 15 : Ewald sphere construction in the reciprocal space showing diffraction process.

Imaging Modes in TEM

TEM can provide almost all data needed to characterize completely the microstructure of material at atomic level. The information derived from TEM is illustrated below :

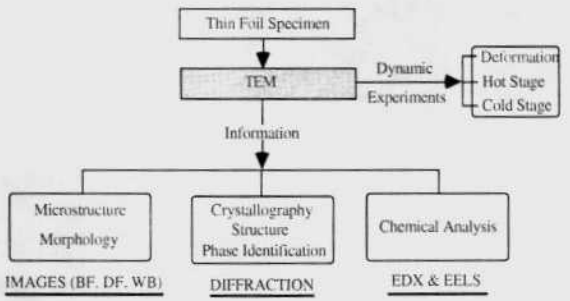

Bright-Field Imaging : is a routine and basic mode used in TEM. The contrast is produced by local elastic strain fields, i.e., defects (dislocation, stacking fault), precipitates etc. The visibility criteria for defect, enable the Burgers vector or displacement vector of defects to be established. Fig. 16a depicts the bright-field (BF) imaging condition while Fig. 16b shows the BF image of bcc nanocrystals precipitation in Fe-Nb-Cu-Si-B amorphous matrix.

Dark-Field Imaging : The DF images are usually produced by tilting the illumination so that diffracted beam aligned parallel to the optic axis of the microscope. This diffracted beam is allowed to pass through the objective aperture and thereby forming the DF image at the image plane. Procedure for forming the DF image is depicted in Fig. 17a and corresponding DF image formed with 110 bcc reflection is shown in Fig. 17b. The DF imaging using specific diffraction spots is a very important and useful technique in analyzing complicated diffraction patterns and in performing quantitative analysis of crystal defects.

Moire' Fringes: Moire' fringes occur when the electron beam successively penetrate two crystalline phases and two closely spaced reflections from the two phases are strongly excited and are both contained in the objective aperture. The Moire' fringes are called parallel Moire' when the corresponding diffracting lattice planes are parallel but differement lattice parameters. The fringe spacing D in a parallel Moire' is;

$$D = (d_1 \times d_2) / |d_1 - d_2|. \qquad \ldots (3.7)$$

where d_1 and d_2 are diffracting lattice planes of the two crystals. It is evident from this relation that the Moire' fringe spacing decreases with increasing lattice mismatch. High contrast imaging of Moire' fringes can be achieved in two beam condition with low index reciprocal lattice vectors.

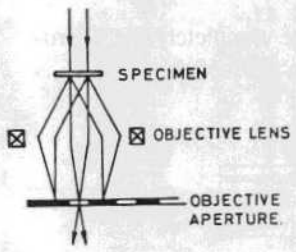

Fig.16: (a) BF imaging where the objective aperture is positioned to allow the direct beam to form the final image; (b) BF image showing bcc nanocrystals in Fe-Nb-Cu-Si-B amorphous matrix.

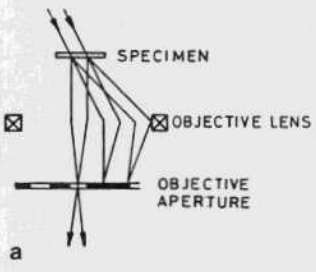

Fig.17: (a) DF imaging where illumination is tilted to select a given diffracted beam; (b) DF image obtained by 110 reflection showing distribution of bcc nanocrystals

Moire' fringes can be very useful to investigate the properties of small precipitates. Precipitate which grow epitaxially to a crystalline matrix may reveal Moire' fringes in TEM images. Commonly epitaxial precipitate phases have lattice parameter differences with the matrix on the order of 1% resulting in Moire' fringe spacings on the order of 10 nm. In such cases Moire' fringe images are of little use for investigating precipitate properties. However there are precipitates that have matrix-precipitates lattice mismatch as high as 30%, and still nucleate and grow epitaxially with the matrix. Moire' fringes in such cases have spacings of about 1 nm which can be utilized to investigate the properties of small precipitates. TEM methods suitable for the investigation of precipitates are summarized in table 3.

Table 3: TEM methods for the investigation of small precipitates

Precipitate properties	*Experimental methods*
Detection limit of precipitate formation	SAED: $>10^{-3}$ volume fraction. Moire': single particle > 1.5 nm dia.
Spatial distribution	BF, DF: inaccurate in the vicinity of grain boundaries precipitate, and other strongly diffracting crystal defects.
	Moire': accurate
Number density	DF: inaccurate if other defects and precipitates introduce matrix strain.
	Moire': can count all particles of dia.> 1.5 nm
Size	BF/DF: Computer simulation of starin contrast (not applicable in vicinity of other ppt. and lattice defects).
	Moire': diameter can be determined within 0.5 nm accuracy.
Shape	BF/DF: computer simulation of strain contrast (if shape can be described by 1 or 2 shape parameters).
	Moire': also irregular shape can be observed.

BF, DF and SAED are more suitable for examining large and more representative sample areas, while the Moire' can only be seen at high magnification (>100,000 x on negative) and in correspondingly small specimen areas. However Moire'

fringe imaging offer more accurate methods for the precipitate properties listed in the table 3.

Lorentz Microscopy : This is an important tool for studies on the micromagnetic structure of thin magnetic films in a TEM. In conventional TEM the domain structure of the specimen can be identified by Fresnel and Foucault techniques. The Fresnel technique reveal domain walls while Foucault technique provide some information on the direction of induction in domains. Figure 18 shows how these modes are implemented in a TEM. Fresnel imaging relies on defocusing the image-forming lens by Δz from specimen plane to delineate regions where the induction direction changes as light or dark narrow bands on uniform background. Foucault imaging gives information on the induction direction within domains through the use of an off-centered aperture in the back focal plane of the imaging lens. This prevents electrons which have been deflected in a particular direction from contributing to the final image. The Foucault imaging mode in a TEM with field emission gun (FEG) electron source greatly enhances the obtained information due to the coherent nature of the electron source. This new imaging mode have been called coherent Foucault (CF) which uses a special aperture to produce magnetic interferograms. Due to the small size of the electron source which means that the illumination in TEM can be considered as a plane wave. Detailed treatment of the imaging of a finite magnetic specimen shows that under certain conditions interference fringes are observed in the final image which run parallel to the local induction direction. The spacing of the fringes, Δs, is given by:

$$\Delta s = h / (eB_o t) \qquad ...(3.8)$$

where h is Planck's constant, e is the unit of electronic charge, B_o is the saturation induction of the magnetic material and t is the film thickness. In standard Foucault imaging, an opaque aperture is used in the back focal plane which produces fringes in domains that deflect electrons through the hole in the aperture. If a phase shifting aperture (50 nm thick Si_3N_4 membrane) is used with a small hole in it such that the central spot in the diffraction pattern lies on the edge of the hole and the spot due to magnetic deflections pass through the Si_3N_4, then fringes are observed in all directions. The aperture material and thickness are chosen such that a phase shift of π is introduced to the electrons which pass through the Si_3N_4.

Examples of CF images (of 30 nm thick permalloy, saturation induction of 1.0 T, patterned by electron beam lithography and lift off techniques into square and rectangular shaped elements) obtained with phase shifting aperture are shown in Fig. 19. They clearly show the induction distribution within each elements. In Fig. 19(a) the elements has a well defined flux closure structure with the do-

mains separated by 90° walls whereas the Fig. 19(b) displays incomplete flux closure. A schematic of the magnetic structure of the elements are shown in Fig. 20. The real time magnetic structure is obtained from single image which is an advantage over standard Foucault imaging where two orthogonal components need to be mapped to give complete information.

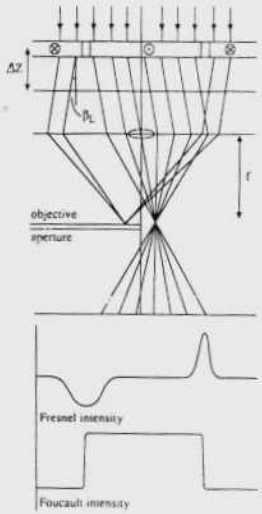

Fig.18: Schematic of Fresnel and Foucault mode of Lorentz microscopy.

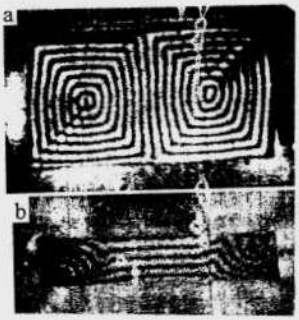

Fig.19: Coherent Foucault (CF) images of 30 nm thick elements in zero applied field produced by a phase shifting aperture. The in-plane dimensions are (a) 4 x 20 μm, and (b) 4 x 0.75 μm.

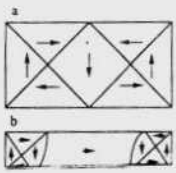

Fig.20: Schematic of the magnetization distribution in the elements shown in Fig. 19.

SCANNING TIP MICROSCOPIES

The generic concept of scanning tip microscopies is much the same as the conventional SEM. Both provide one-to-one mapping between a point sampling of some physical property of a probe-sample surface interaction and a corresponding point in an image. Correspondence between points on the sample surface and image points is achieved by synchronizing the image generation process with probe motion. The major difference between tip microscopy methods are that no lenses are used, probe motion relative to the specimen is produced mechanically, and probe is a solid material.

The variation of the tip-specimen interaction with spacing and properties of the phenomena involved determine the dynamic range of the techniques, the vertical resolution obtainable, and often is a factor in determining lateral resolution. The basic idea behind scanning tip microscopies is quite simple as illustrated in Fig. 21. This aspect of microscopies is summarized in table 4.

Table 4: Scanning Tip Microscopies

Microscopy	*Transducing Parameter*	*Parameter variation with tip-specimen spacing (S)*
Topografiner	Field-emission Emitter-anode Potential, V	$V(S) = c_1F + c_2FS^{1/2}$
STM	Tunneling Current, I	$I(S) = c_3V \exp(-c_4\phi^{1/2}S)$
AFM	Van der Waals Force, F	$F(S) = c_5S^{-3}$
SCaM	Capacitance, C	$C(S) = c_6 \log S$
Scanning Thermal	Tip Temperature, T	$T(S) = c_7S^P$; $P>2$
NSOM or NFOS	Near-Field Optical Electrical Field Energy Density, $\|E\|^2$	$\|E\|^2 = c_8(S/a)^{-3.7}$

Where F = Field-strength at emitter surface to maintain constant current, ϕ = Mean tunneling barrier height, V = Bias voltage, a = Radius of near-field aperture, and c_i = Constants.

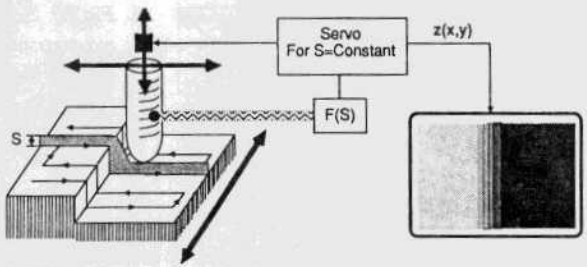

Fig. 21: Basic operation of scanning tip microscope.

Scanning Tunneling Microscopy (STM)

The invention of scanning tunneling microscopy (STM) which won the 1986 Nobel Prize in Physics has allowed one to image atoms on the surface of a metal or semiconductor by scanning fine tip (of dia. ~ 1000 Å) in a controlled fashion very close (2Å) to the sample surface. In STM, the tip to sample distance is controlled by measuring the tunneling current, i.e., the current that flows between the tip and sample when a voltage is applied between them (which changes very rapidly with this distance) and using piezoelectric transducer to precisely position the tip in three dimensional space to 1Å accuracy. The STM respond to variation in the electron density of states of the sample surface.

Atomic Force Microscopy (AFM)

As in STM, the same piezoelectric positioning and control concepts were used to measure other physical interactions rather than tunneling current to control the tip-sample spacing. The force is measured by first exciting a tungsten (or other) tip near its mechanical resonance using a piezoelectric transducer. Typically the resulting amplitude of tip vibration might be around 10Å. As the tip approaches the sample, it "feels" a force due to the presence of the sample. This interaction might be due to magnetic, electro-static or van der Waals forces depending on the particular tip/sample configuration chosen. The action of these forces on the tip (which decreases as the tip-sample distance is increased) alter its resonance frequency. Since the tip is driven at constant frequency, this shift manifests itself as a change in the tip vibration amplitude. This change is measured by using a sensitive laser heterodyne probe and then compared with a reference signal in order to generate a feedback signal which controls the tip-sample spacing (so as to maintain a constant amplitude of tip vibration) as the tip is rastered across the sample to record an image. With this technique, force down to 10^{-12} N (i.e., less than typical interatomic forces) and force gradient down to 10^{-4} N/m can be measured.

Scanning Capacitance Microscopy (SCaM)

By applying AC voltage on the tip, it becomes possible to measure electrostatic forces due to applied or induced charges. Effective capacitance of 10^{-22} F can be detected which means that the charge variations caused by single electron can be imaged.

Scanning Thermal Probe

Finally, a thermal probe can map out temperature variation on a surface with 1000 Å spatial resolution and milli-degree sensitivity. This, coupled with a tunable optical heating source makes it possible to do optical absorption spectroscopy on a microscopic scale, thereby making it possible to identify chemical species with 1000 Å lateral resolution.

CONCLUDING REMARK

Improvement in known materials and development of new ones should be based on understanding of the relations between microstructure and properties. Electron microscopy is by far the most powerful experimental tool for such developments. It reduces the requirements for empirical testing and therefore opens the most economic path to provide our civilization with better materials. The main benefits to society arises from the advances in scientific understanding through application in the fields of Materials science, Biology and Medicine.

BIBLIOGRAPHY

(1) M. Born and E. Wolf, Principles of optics, Pergamon Press, Oxford (1964).

(2) J. H. Richardson, Optical Microscopy for materials science, Marcel Dekker, New York (1971).

(3) S. Tolansky, Multiple beam interference microscopy of metals, Academic Press, London (1970).

(4) S. Tolansky, Microstructures of surfaces using interferometry, Edward Arnold, London (1968).

(5) P. B. Hirsch, A Howie, R. B. Nicholson, D. W. Pashley and M. J. Whelan, Electron microscopy of thin crystals, Butterworth, London (1965).

(6) J. A. Stroscio and W. J. Kaiser (Eds.), Scanning tunneling microscopy, Academic Press, New York, (1993).

(7) J. C. Russ, Computer assisted microscopy, Plenum Press, New York (1990).